Modelling Wind Turbine Wakes in Complex Terrain

J. M. Prospathopoulos, e-mail: jprosp@cres.gr
E. S Politis, e-mail: vpolitis@cres.gr
P. K. Chaviaropoulos e-mail: tchaviar@cres.gr
Centre of Renewable Energy Sources, Wind Energy Department
19 km Marathonos Ave., GR19009, Pikermi, Attiki, Greece

Abstract:

Existing engineering-type models for wakes have been developed and calibrated for flat terrain applications. However to consider the effects of the atmospheric boundary layer in a complex terrain environment, including flow separation and wind rose narrowing, requires the application of advanced methods. A method of modeling the wind turbine wakes using a Navier–Stokes solver along with the k–ω turbulence model is presented in this paper. Wind turbines are modelled as momentum absorbers, by means of their thrust coefficient. Application is made for two ideal, Gaussian, hill configurations, one axisymmetric 3D and one quasi-3D, for various turbulence and wind direction conditions. The numerical predictions for the hill configurations are compared with those in flat terrain.

Keywords: wind turbines, complex terrain wake deficit, Navier–Stokes

1 Introduction

Wind turbine wakes have attracted a lot of attention by the research community since they are characterized by momentum deficits and increased turbulence levels, which contribute to reduced power outputs of a wind farm and increased loading. The issue is magnified by the need for installing the machines as closely as possible to each other, trying to maximize the exploitation of the land in wind energy installations, especially in complex terrain. Similar restrictions hold to off-shore wind installations.

The need for accurate model of the wakes has been recognized for many years and various models have been developed to simulate the wind turbine wakes. Most of them refer to flat terrain installations.

The simplest approach is that of a kinematic (or explicit) model based on self-similar velocity deficit profiles obtained from experimental and theoretical work on co-flowing jets. Lissaman [1] and Voutsinas et al. [2] used the profiles proposed by Abramovich [3], whereas Vermeulen [4] used a Gaussian type of profile similar to that of Abramovich. Later, Kiramoudis and Maroulis [5] developed a “short-cut model of wind park efficiency”, providing simple analytical expressions of the efficiency as a function of the wind farm and turbine characteristics. In all above studies the reference value of the velocity deficit at each section has been obtained from global momentum conservation with the exception of Voutsinas et al. [2], who used mass conservation.

Larsen et al. [6] and Madsen [7] from RISØ National Laboratory developed simple analytical models, where the flow is assumed axisymmetric and a single self-similar profile is assumed for the whole wake. In these models, the velocity deficit and the turbulence decay with downstream distance x as a function of $x^{-2/3}$ and $x^{-1/3}$, respectively, whilst the wake width increases as a function of $x^{1/3}$. These exponential decay dependencies are derived, using a boundary layer approximation with the assumption of self similar axisymmetiric velocity profiles and zero pressure gradient, They obtained good agreement with empirical relations in all cases that the downstream distance is larger than two diameters.

A more advanced approach is that of the field (or implicit) models which calculate the flow magnitudes at every point of the flow field giving a better insight into the physical mechanisms that govern the wake development. Sforza [8] described the wake using the parabolic approximation for the linearized momentum equation in the main flow direction. Agreement with small-scale experiments was within 10% for the velocity deficit, except for cases of high thrust loading, for which the error reached 20%. Taylor [9]

used a two-dimensional boundary layer approximation in neutrally stratified atmosphere. His predictions were found in reasonable agreement with experimental results, however, the linear superposition in the case of several wind turbines made its model inapplicable to wind farms. Ainslie [10] developed a parabolic eddy viscosity model (EVMOD) which assumes axisymmetric wake flow and ignores the ground effects and the variations with height. Its predictions were in reasonable agreement with wind tunnel experiments. Crespo et al. [11] developed the UPMWAKE model where atmospheric stability and roughness are taken into account. It is a parabolic approximation method, using the SIMPLE algorithm of Patankar and Spalding [12], in which the turbulent stresses are modelled through the k–ε model. The predictions of UPMWAKE model were validated against the ones using the commercial CFD PHOENICS code and wind tunnel and full-scale experiments. Comparison was good with the exception of the initial wake region, where the predicted velocity deficits were smaller than the measured ones. Based on the model of Ainslie [10], Garrad Hassan & Partners Ltd. developed the EVFARM code described by Tindal [13]. It is an axisymmetric Navier–Stokes solver with eddy-viscosity closure, initiated at a distance of two diameters behind the rotor using an empirical wake profile. The eddy-viscosity is defined using the turbulence intensity in the wake. The comparison of UPMWAKE and EVFARM models with the wind tunnel measurements of Hassan [14] showed good agreement for the velocity deficit, which was underestimated by 2% and 3% respectively. The turbulence intensity was overestimated by 11% by EVFARM and underestimated by 17% by UPMWAKE.

One possible reason for the differences between the predictions and measurements is the uncertainty in the definition of the initial velocity deficit. Zervos et al. [15] used a vortex particle method to relate initial wake development with the aerodynamics of the rotor. The advantage is that no initial data are needed to start the calculations; however the validity of the solution is limited to the initial expansion region where diffusion effects can be neglected. Voutsinas et al. [16] extended this model dividing the wake into the rotor region, the near-wake region and the far-wake region, and applied a vortex-particle method in the rotor region, a field model in the near-wake region and self-similar expressions in the far-wake region. The method gave good agreement with the experimental results of the Nibe wind turbines reported in [17], and less good but still reasonable agreement with the experiment of Alsvik wind farm [18].

ECN developed the WAKEFARM program which is a slight modification of the UPMWAKE model. Empirical corrections were added to the standard momentum theory used for the near wake modelling [19]. Apart from its semi-analytical engineering-type models [6], [7] RISØ National Laboratory developed a CFD actuator disk code interfaced to an aeroelastic code [20], thus enabling a detailed modelling of the turbine as well as of the flow field. University of Oldenburg developed the FLaP wind farm model [21], which is also an axisymmetric implementation of the Ainslie wake model [10], solving the momentum and continuity equations with an eddy-viscosity closure. The near wake length is calculated after Vermeulen [4] taking into account ambient, rotor generated and shear generated turbulence intensity. Robert Gordon University developed a CFD fully elliptic turbulent 3D Navier–Stokes solver with k–ε turbulence closure based on the axisymmetric model of Voutsinas et al. [16]. Initial data required to start the calculations are the velocity and turbulence intensity profiles in the atmospheric boundary layer upstream the rotor. The wind turbine is approximated by a semi-permeable disk to simulate the pressure drop across the real rotor disk.

The last five models along with the analytical model of Uppsala University which is based on the Taylor approximation [9] were compared with the experimental data of the Vindeby and Bockstigen wind farms [22]. Almost all models overestimated the wake effects for near neutral atmospheric conditions. The predictions presented faster wake recovery for higher ambient turbulence intensity and thrust coefficient. Their performance in predicting power output at Bockstigen was considered satisfactory.

Sørensen and Shen [23] developed a 3D Navier–Stokes solver with a so-called actuator line technique in which loading is distributed along lines representing the blade forces. The loading is determined iteratively using a blade-element approach and tabulated airfoil data. Predictions were found in good agreement with measurements for a 500 kW Nordtank wind turbine equipped with three LM19.1 blades. Finally, Frandsen et al. [24] proposed an

analytical model for both small and large offshore wind farms. It encompasses three regimes, the first simulates the expansion of multiple-wake flow in a single row, the second materializes the merging of wakes from neighbouring rows and the third refers to the far field when the flow is in balance with the boundary layer. The model is going to be verified / calibrated by means of the experimental data at the large offshore wind farms in Horns Rev and Nysted.

From the preceding review of the available wake models, it is obvious that all methods focus on wake modelling in flat terrain. Trying to enhance the knowledge for the wake behaviour in complex terrain, in the present paper a full 3D Navier–Stokes solver, along with *k–ω* turbulence closure suitably modified for atmospheric conditions, is applied for wake simulation of a wind turbine positioned at a hill top. The rotor disk is simulated as a momentum sink through the actuator force which is related to a constant over the rotor area thrust coefficient. Simulations are performed for an axisymmetric and a quasi-3D Gaussian hill terrain and for various ambient turbulence intensity and wind inflow conditions.

Recognizing that it is not possible to conduct full scale measurements at complex terrain, only simulations in wind tunnel environment have been conducted in the past [25], the full 3D Navier–Stokes modelling of the flow characteristics in complex terrain can constitute the basis for the assessment of the simpler engineering wake models regarding the prediction of velocity deficit and turbulence intensity.

2 Methodology

2.1 The Navier–Stokes Algorithm

The governing equations are numerically integrated by means of an implicit pressure correction scheme, where wind turbines (W/Ts) are modelled as momentum absorbers by means of their thrust coefficient [26]. A matrix-free algorithm for pressure updating is introduced, which maintains the compatibility of the velocity and pressure field corrections, allowing for practical unlimited large time steps within the time integration process. Spatial discretization is performed on a computational domain, resulting from a body-fitted coordinate transformation, using finite difference/finite volume techniques. The convection terms in the momentum equations are handled by a second order upwind scheme bounded through a limiter. Centred second order schemes are employed for the discretization of the diffusion terms. The Cartesian velocity components are stored at grid-nodes while pressure is computed at mid-cells. This staggering technique allows for pressure field computation without any explicit need of pressure boundary conditions. A linear fourth order dissipation term is added into the continuity equation to prevent the velocity-pressure decoupling. To accommodate the large computational grids needed in most applications with a fair discretization of the topography at hand, a multi-block version of the implicit solver has been developed.

2.2 Turbulence Closure

The most commonly used turbulence closure in Reynolds–averaged Navier–Stokes solvers are the *k–ω* and *k–ε* models. Dealing with atmospheric flows, the coefficients of the models should be suitably modified since they have been calibrated in aerodynamic (wind tunnel) flows. The standard coefficients of the two models are:

$$\alpha = 5/9, \quad \beta = 3/4, \quad \beta_* = 0.09, \quad \sigma = 0.5, \quad \sigma_* = 0.5 \tag{1}$$

(for k–ω [27]) and

$$C_{\varepsilon 1} = 1.44, \quad C_{\varepsilon 2} = 1.92, \quad C_\mu = 0.09, \quad \sigma_k = 1.0, \quad \sigma_\varepsilon = 1.3 \tag{2}$$

(for k–ε [28]).

The correspondence between the two models indicates that $C_\mu = \beta_*$. The coefficients C_μ, β_* are established for atmospheric flows using the condition for the logarithmic layer at the wall,

$$k = u_*^2 / \sqrt{\beta_*} \tag{3}$$

and the fact that u_*^2 / k in neutral atmosphere has been measured between 0.17 and 0.18 [29],[30],[31]. Therefore:

$$\beta_* = C_\mu = 0.033 \tag{4}$$

The range of values for von Karmann's constant K is 0.37–0.41 [32]. For light winds over flat terrain, where roughness is small, measurements suggest K=0.41 [33], which is the value adopted in this paper.

For decaying homogeneous, isotropic turbulence, the simplified equations for *k, ε,* and *ω* lead to the following asymptotic

solutions:

$$k \sim t^{-\beta_* / \beta}, \quad k \sim t^{1/1-C_{\varepsilon 2}} \tag{5}$$

For such conditions, the experimental (aerodynamic) observations of Townsend [34] indicate that $k \sim t^{-n}$, where $n = 1.25 \pm 0.06$. Choosing $n = 1.2$ sets the ratio $\beta_* / \beta = 1 / (C_{\varepsilon 2} - 1)$ at the lower end of the range of accepted values, which implies:

$$\beta = 0.0275, \quad C_{\varepsilon 2} = 1.83 \tag{6}$$

However we must stress that to the knowledge of the authors there are no similar atmospheric observations to enable the correct recalibration of the models for atmospheric flows, which is indeed needed.

Finally, in the limiting case of an incompressible constant-pressure boundary layer, the mean momentum and k, ω (or ε) equations are simplified [27]. The constraint imposed to the solution of these equations provides the following unique relation between the von Karmann's constant and the various closure coefficients:

$$\alpha = \beta / \beta_* - \sigma K^2 / \sqrt{\beta_*}, \quad C_{\varepsilon 1} = C_{\varepsilon 2} - K^2 / (\sqrt{C_\mu}\sigma_\varepsilon) \tag{7}$$

By using the standard values of coefficients σ and σ_ε, Eq. (7) yields:

$$\alpha = 0.3706, \quad C_{\varepsilon 1} = 1.12 \tag{8}$$

So, the modified closure coefficients of the k–ω and k–ε models for atmospheric conditions are:

$$\alpha = 0.3706, \quad \beta = 0.0275, \quad \beta_* = 0.033, \quad \sigma = 0.5, \quad \sigma_* = 0.5 \tag{9}$$

and

$$C_{\varepsilon 1} = 1.12, \quad C_{\varepsilon 2} = 1.83, \quad C_\mu = 0.033, \quad \sigma_k = 1.0, \quad \sigma_\varepsilon = 1.3 \tag{10}$$

2.3 Numerical Aspects

The governing equations are discretized and solved in their non-dimensional form, using a reference length and velocity the W/T rotor diameter, D, and the free stream velocity, U_∞, respectively. The dimensions of the computational domain are extended sufficiently so that the flow is not restricted by its numerical boundaries. In each case, the x, y-axes are selected so that their origin coincides with the W/T position. The distribution of grid-lines is kept the same for all examined cases. In both horizontal directions, the grid size is constant, equal to 0.05D, in the range ±0.55D (around the W/T), and increases outwards, following a geometrical progression, until the maximum dimension of the domain is reached (see Figure 1). In the vertical direction, the first three grid-lines are positioned close to the ground at heights 0.01, 0.03 and 0.05D respectively. From 0.05D up to a height of 1.55D the grid size is kept constant, equal to 0.05D, and then increases following a geometrical progression up to the maximum height of the domain. In this way, a fine mesh is constructed in the area of the W/T rotor disk.

If the wind direction is not parallel to the x-axis, the rotor disk is rotated by a yaw angle to remain perpendicular to the flow. This angle is the velocity direction at the W/T's rotor centre calculated from the simulation without W/T. In such a case the horizontal grid mesh is modified, so that the grid lines are aligned with the plane of the yawed rotor disk.

The inflow wind velocity profile follows the logarithmic law:

$$U_x = \frac{u_*}{K} ln(z / z_0), \tag{11}$$

where u_* is the friction velocity, K is the von-Karmann constant and z_0 is the roughness length. In case the wind is not aligned with x direction, Eq. (11) takes the form:

$$U_x = \frac{u_*}{K} ln(z / z_0) \cos(\alpha_w), \quad U_y = \frac{u_*}{K} ln(z / z_0) \sin(\alpha_w), \tag{12}$$

where α_w is the wind direction relative to x-axis. The friction velocity is related to the roughness through:

$$u_* = K / ln(\delta / z_0), \tag{13}$$

with δ being the assumed atmospheric boundary layer thickness and $U_x(\delta) = 1$. The inflow k and ω profiles are given by the relationships:

$$k = u_*^2 / \sqrt{\beta_*}, \quad \omega = u / \left(\sqrt{\beta_*} K z\right). \tag{14}$$

On the terrain surface, the non-slip condition yields zero velocity. The Cartesian velocity components are specified at the upper far-field boundary ($U_x = 1, U_y = 0, U_z = 0$). Neumann velocity conditions are imposed at the outflow and the side boundaries. For the k and ω boundary conditions a similar approach is followed. Here, however, Neumann conditions are imposed at the inlet plane as well, allowing k and ω to adapt themselves to the prescribed boundary conditions.

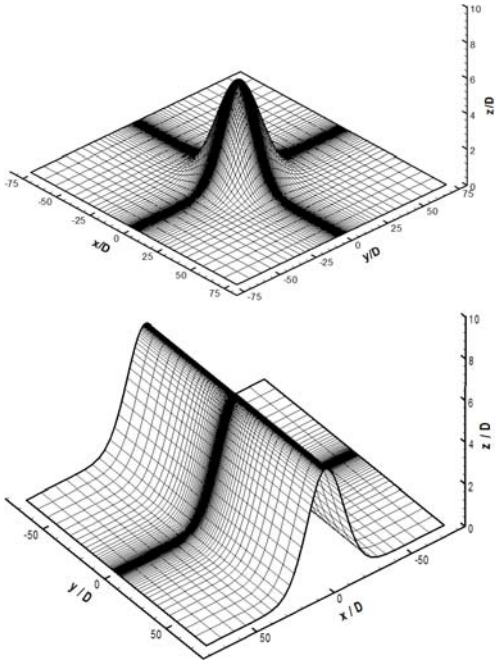

Figure 1: Digitized terrain of the axisymetric (upper) and quasi-3D (lower) Gaussian hill.

3 Description of test cases

The idealized simulation of a single wake in the case of a Gaussian hill has been selected as fundamental for the comparison of the wake characteristics between flat and complex terrain. The conclusions deduced from the analysis of the axisymmetric and quasi-3D Gaussian hill can be extended to more complex terrain where the irregularities of the topography are seen as separate hills.

The Gaussian quasi-3D hill geometry is defined by the relationship:

$$z = h\, exp\left[-0.5\left(\frac{x}{\sigma}\right)^2\right],\ \sigma = L/1.1774\ ,\ (15)$$

where *x, z* are the horizontal and vertical coordinates, *h* is the height of the hill and *L* is defined as $x(z = h/2)$. In the case of the axisymmetric hill, the quantity $\sqrt{x^2 + y^2}$ replaces *x* in Eq. (15). The axisymmetric and quasi-3D hill terrains derived from equation (15) for *L*=1750 m are shown in Figure 1. The configuration investigated corresponds to *h*=700 m and *L*=1750 m, which denotes a mean slope of 0.4. The grid size was about 750000 nodes for the two hill cases with 101 nodes placed in the streamwise and the lateral directions, and 73 nodes in the vertical direction. The disk rotor was discretized using 21 nodes. The flat terrain cases were discretized using 309000 nodes.

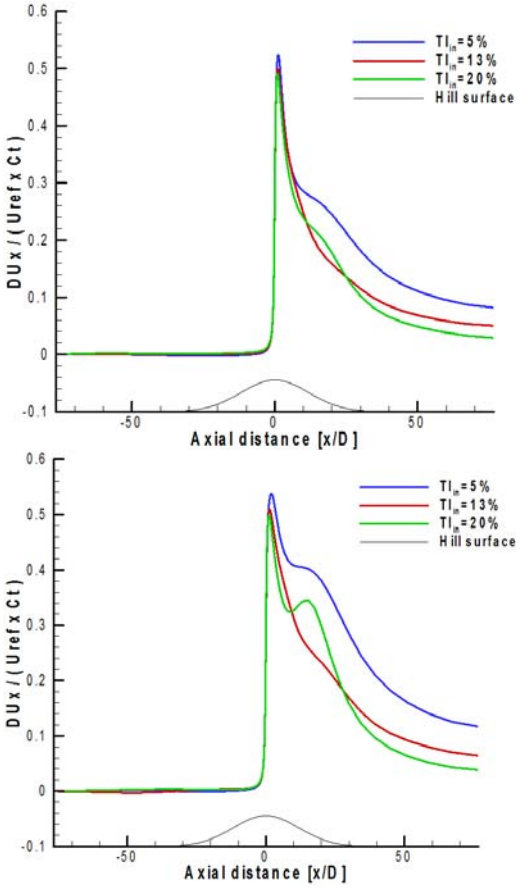

Figure 2: Wind speed deficit along $y = 0$ line at hub height for various values of inlet turbulence intensity for axisymmetric (upper) and quasi-3D hill (lower).

The different configurations are simulated with one W/T placed at hilltop and without. The simulations without W/T are needed to provide the value of wind speed at the W/T position for the calculation of the actuator disk force as well as the reference velocity field for the evaluation of the wind speed deficit. After the wind speed at hilltop, hub height, has been predicted in the absence of W/T, its thrust coefficient C_t is estimated using a $C_t(V)$ curve provided by the application of a Boundary Element Method under flat terrain conditions for a range of constant wind speeds.

The W/T is a paper case 5 MW machine with a diameter of 126 m and 90 m hub height. The inflow wind speed profile is assumed logarithmic with 500 m boundary layer height and 10 m/s wind speed at hub height. Three different levels of inlet turbulence intensity TI_{in} at hub height, 5%, 13% and 20%, are examined. The different levels of TI_{in}

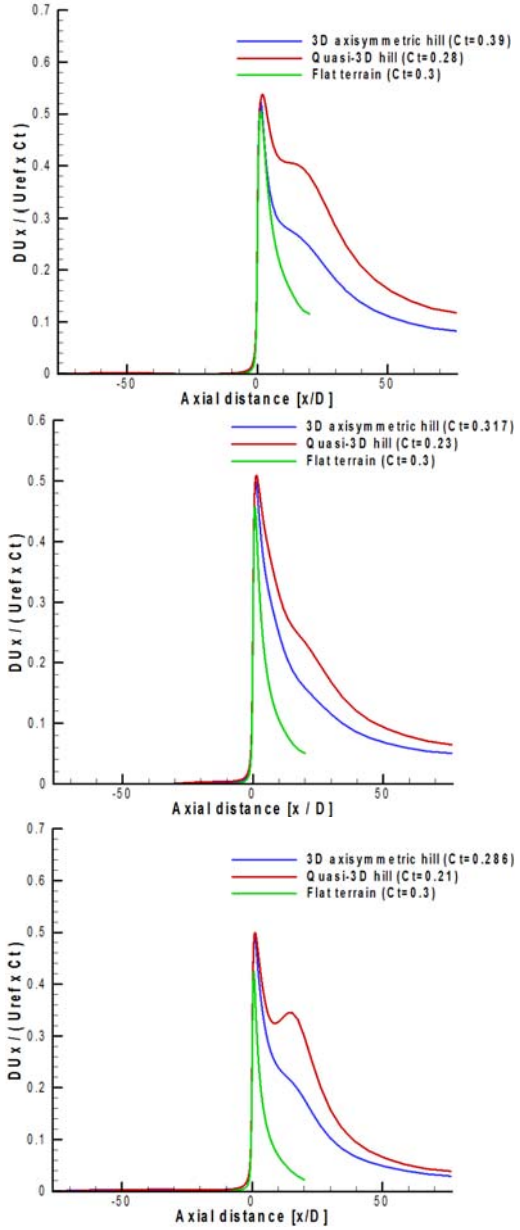

Figure 3: Comparison of the velocity deficit at hub height among the axisymmetric, the quasi-3D hill and flat terrain. Upper: TI_{in} = 5%. Middle: TI_{in} = 13%. Lower: TI_{in} = 20%.

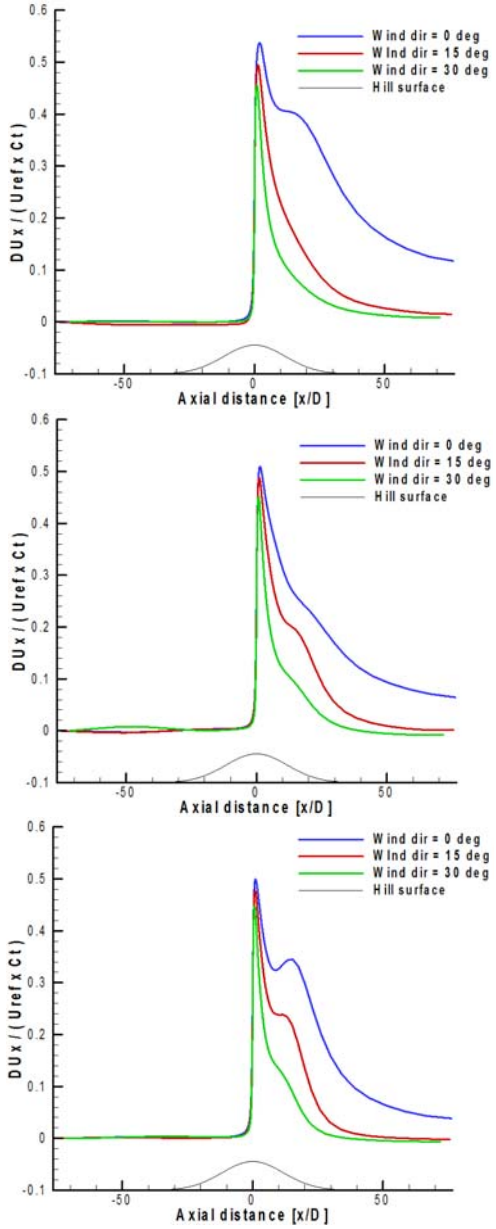

Figure 4: Velocity deficit at hub height above the quasi-3D hill, for various wind directions Upper: TI_{in} = 5%. Middle: TI_{in} = 13%. Lower: TI_{in} = 20%.

correspond to different values of roughness length ($2.29\ 10^{-7}$, 0.0445 and 0.639 m respectively, see Appendix) and subsequently to different inflow wind velocity profiles. For the quasi-3D hill case, the effect of the wind direction is also investigated through simulations for three different wind directions, 0^o, 15^o and 30^o.

4 Results and Discussion

The velocity deficit is calculated with reference to the predictions without W/T, using the relationship:

$$\frac{DU_x}{U_{ref} \times C_t} = \frac{U_{ax}(\text{without W/T}) - U_{ax}(\text{with W/T})}{U_{ax}(\text{without W/T}) \times C_t} \qquad (15)$$

In the above definition the velocity field predicted from the simulation without W/T is used as the reference to calculate the deficit. U_{ax} stands for the U_x velocity for 0^o wind direction or the total horizontal velocity $\sqrt{U_x^2 + U_y^2}$ when the wind direction is 15^o or 30^o.

The velocity deficit is presented in Figure 2 for the 3D axisymmetric and the quasi-3D hills for

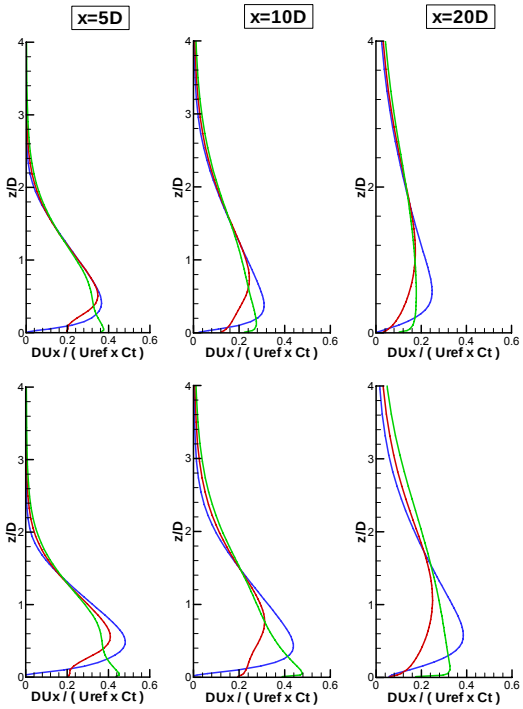

Figure 5: Vertical profiles of velocity deficit at 5, 10 and 20*D* downstream the W/T for varying inlet turbulence intensity. Blue line:5%, green line:13%, red line: 20%. Upper: axisymmetric, Lower: quasi-3D hill.

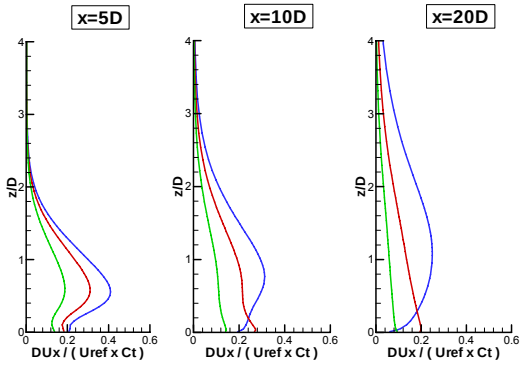

Figure 6: Vertical profiles of velocity deficit at 5, 10 and 20*D* downstream the W/T for various wind directions of quasi-3D hill. Blue line: 0°, red line:15°, green line: 30°.

different levels of TI_{in}. One important conclusion drawn from the figure is that in both hill cases the deficit remains significant at long distances downstream the W/T (even greater than 40*D*). The decay rate is slower for the quasi-3D hill. On the contrary, in the flat terrain case, the deficit has already been practically negligible at 20*D*.

The comparison between hill and flat terrain cases is shown in Figure 3. The increase of the turbulence level results in a faster flow

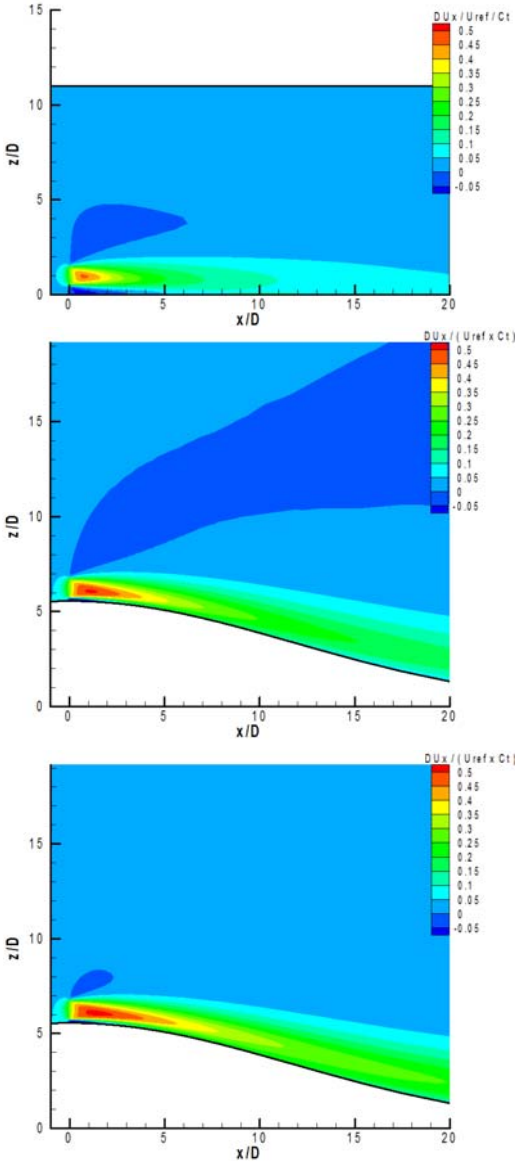

Figure 7: Velocity deficit contours at plane $y = 0$ for TI_{in} =13%. Upper: flat terrain. Middle: axisymmetric hill. Lower: quasi-3D hill.

recovery at long distances as expected. However, it is noticeable that the wind speed deficit at hub height is not always monotonously decreasing. This is mainly observed in the quasi-3D case and is more pronounced for the $TI_{in} = 20\%$ case.

Another important remark is the drastic effect of the wind direction on the decay rate of deficit. As depicted by Figure 4, a change in the wind direction from 0 ° to 30 ° significantly increases the decay rate. At 30° wind direction, the decay rate of deficit is comparable to that of flat terrain.

The vertical velocity deficit profiles are plotted in Figure 5 at increasing distance downstream

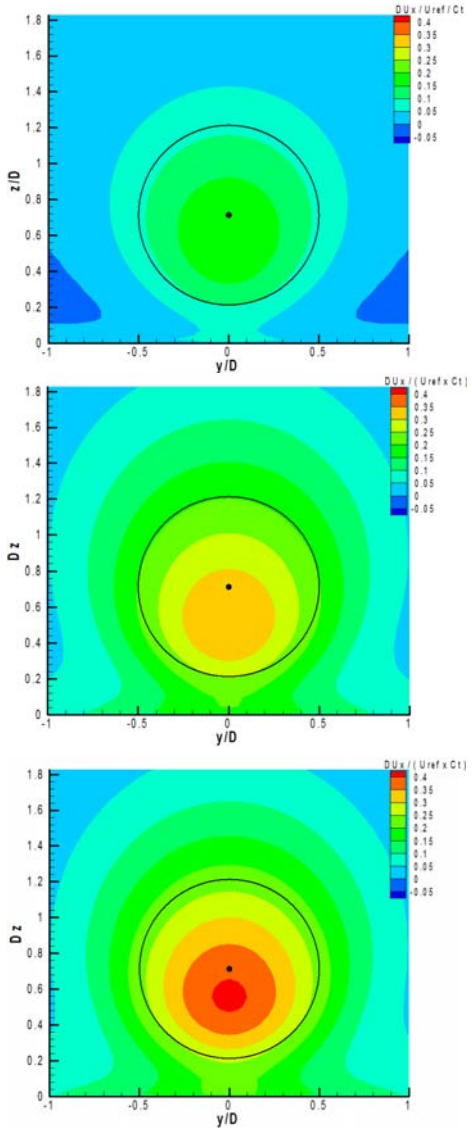

Figure 8: Velocity deficit contours 5*D* downstream the W/T for TI_{in} = 13%. Upper: flat terrain. Middle: axisymmetric hill. Lower: quasi-3D hill.

the W/T. A straightforward observation is the modification of the wake geometry with turbulence, especially in the $TI_{in} = 20\%$ case, which is responsible for the aforementioned non-monotonous variation of the axial deficit. The height of the maximum velocity deficit reduces with increasing TI_{in} and for TI_{in} = 20% is located close to the ground. Another remark is that the predicted velocity deficit keeps higher values in the quasi-3D hill terrain, denoting a slower decay rate which was also seen in the axial deficit variation.

The significant effect of the wind direction on the deficit is confirmed by the profiles of Figure 6. The height of the maximum deficit remains constant; its level however attenuates fast as the wind direction changes from 0^o to 30^o. For the 30^o case, the velocity deficit is practically negligible after 20*D*.

A more visual representation of the deficit features is made using the contour plots. In Figure 7, the deficit contours at the plane $y = 0$ are compared for the two hills and the flat terrain case. The wake evolution at long distances in both hill cases, and particularly in the quasi-3D case, contrasts the quick vanishing in the flat terrain case.

A detailed illustration of the wake geometry can be made by focusing on the region behind the W/T at a plane parallel to the rotor disk. In Figure 8, the deficit contours are presented at 5*D* downstream the W/T for $TI_{in} = 13\%$. In the flat terrain case, the wake centre is about 0.1*D* lower than hub height at 5*D* downstream. In the axisymmetric and the quasi-3D hill cases, the height difference between wake centre and hub becomes about 0.2*D* at 5*D* downstream.

5 Conclusions

The wake characteristics of a paper case 5 MW wind turbine placed on the top of a Gaussian hill were investigated and compared with the respective characteristics in flat terrain. Two different hill geometries were examined, a 3D axisymmetric and a quasi-3D one. The effects of the hill terrain, the turbulence intensity level and the wind direction on the wake characteristics were assessed. The basic conclusions drawn from the numerical analysis are summarized below.

The change of the inlet turbulence intensity level, which is equivalent to a change in roughness, affects the shape of the velocity boundary layer. An increase in the inlet turbulence produces higher accelerations at the hill top and higher decelerations at the lee side of the hill. This effect is reinforced by the W/T presence and is more pronounced in the quasi-3D hill. As a result, the increase of the turbulence level causes a decrease in the thrust coefficient value of the W/T, implying a weaker velocity deficit.

In both hill cases the velocity deficit remains significant at 20*D* downstream the W/T, and in some cases even at 40*D* ($TI_{in} = 5\%$). On the contrary, in the flat terrain case, the deficit has already been practically negligible at 20*D*. The decay rate is slower for the quasi-3D hill.

The increase of the turbulence level results in a faster flow recovery at long distances as

expected. However, the wind speed deficit at hub height is not always monotonously decreasing. This is a result of the wake geometry modification when the turbulence level changes, which is more pronounced in the quasi-3D geometry for the highest turbulence level ($TI_{in} = 20\%$).

In the flat terrain case, the wake centre is about 0.1*D* lower than hub height at 5*D* downstream. In the axisymmetric and the quasi-3D hill cases, the height difference between wake centre and hub is larger, about 0.2*D* at 5 diameters downstream.

The effect of the wind direction on the decay rate of deficit is drastic. A change in the wind direction from 0^o to 30^o increases the decay rate in such a degree that it becomes comparable to that of flat terrain. For the 30^o case, the velocity deficit is practically negligible after 20*D*. In the near wake, the height of the maximum deficit does not change with wind direction.

Acknowledgements

This work was partly by the European Commission under contract SES6 019945 (UPWIND Integrated Project) and by the Greek Secretariat for Research and Technology.

References

[1] Lissaman, P. B. S., "Wind Turbine airfoils and rotor wakes," in D. A. Spera (ed.), *Wind Turbine Technology*, ASME Press, New York, 1994, pp. 283-323

[2] Voutsinas, S. G., Rados, K. G. and Zervos, A., "On the Analysis of Wake Effects in Wind Parks," *Wind Engineering*, 1990, 14, pp. 204-219

[3] Abramovich, G. N., *The Theory of Turbulent Jets*, MIT Press, Cambridge, MA, 1963

[4] Vermeulen, P. E. J., "An Experimental Analysis of Wind Turbine Wakes," *Proceedings of 3rd Int. Symposium on Wind Energy*, 1990, 14, pp 431-450

[5] Kiranoudis, C. T. and Maroulis, Z. B., "Effective Short-cut Modelling of Wind Park Efficiency," *Renewable Energy*, 1997, 11, pp. 439-457

[6] Larsen, G. C., Hojstrup, J. and Madsen, H. A., "Wind Fields in Wakes," Proceedings of 1996 EWEC, Göteborg, pp. 764-768

[7] Madsen, H. A. A., *Proceedings of IEA Joint Action, Aerodynamics of Wind Turbines 13th Symposium*, Stockholm, 1999

[8] Sforza, P. M., Stasi, W. and Smorto, M., "Three-dimensional Wakes of Simulated Wind Turbines," *AIAA Journal*, 1981, 19, pp. 1101-1107

[9] Taylor, P. A., "On Wake Decay and Row Spacing for WECS Farms," *Proceedings of 3rd International Symposium on Wind Energy Systems*, Lyngby, 1980, pp. 451-468

[10] Ainslie, J. F., "Calculating the Field in the Wake of Wind Turbines," *J. Wind Engng. Ind. Aerodyn.*, 1988, 27, pp. 213-224

[11] Crespo, A., Manuel, F., Moreno, D., Fraga, E. and Hernández, J., "Numerical Analysis of Wind Turbine Wakes," *Proceedings of Delphi Workshop on Wind Energy Applications*, Delphi, 1985, pp. 15-25

[12] Patankar, S. V. and Spalding, D. B., "A Calculation Procedure for Heat, Mass and Momentum Transfer in Three-dimensional Parabolic Flows," *Int. J. Heat Mass Transfer*, 1972, 15, pp. 1787-1806

[13] Tindal, A., Dynamic Loads in Wind Farms, Final Technical Report, *CEC Project JOUR-0084-C*, 1993

[14] Hassan, U., A., Wind Tunnel Investi-gation of the Wake Structure Within Small Wind Farms, ETSU Report WN5113, 1993

[15] Zervos, A., Huberson, S. and Hemon, A., "Three-dimensional Free Wake Calculation of Wind Turbine Wakes," *J. Wind Engng. Ind. Aerodyn.*, 1988, 27, pp. 65-76

[16] Voutsinas, S. G., Rados, K. G. and Zervos A., "Wake Effects of the Rotor Geometry on the Formation and the Development of its Wake," *J. Wind Eng. Ind. Aerodyn.*, 1992, 39, pp. 293-301

[17] Taylor, G. J., Wake Measurements on the Nibe Wind Turbines in Denmark. Part 2: Data Collection and Analysis, *Final Report, CEC Contract EN3W.0039.UK(H1)*, National Power, London, 1990

[18] Magnusson, M., Rados, K. G. and Pothou K. P., "Wake Effects in Alsvik Wind Park: Comparison Between Measurements and Predictions," *Proceedings of 1996 EWEC*, Göteborg, 1996, pp. 769-772

[19] Schepers, J. G., Wakefarm, Nabijzog model en omgestoord windsnelheisveld, Technical Report ECN-98-016, 1998 (in Dutch)

[20] Larsen, G. C., (ed.), Carlén, I. and Schepers, G. J., *European Wind Turbine Standards II. Project Results*, Technical Report ECN-C--99-073, 1999

[21] Lange, B., Waldl, H.-P., Barthelmie R., Guerrero, A. G. and Heinemann, D., "Modelling of Offshore Wind Turbine Wakes with the Wind Farm Program FLaP," *Wind Energy*, 2003, 6, pp. 87-104

[22] Rados, K., Larsen, G., Barthelmie, R., Sclez, W., Lange, B. and Schepers, G., "Comparison of Wake Models with Data for Offshore Wind Farms," *Wind Engineering*, 2001, 25, pp. 271-280

[23] Sørensen, J. N., and Shen, W. Z., "Numerical Modelling of Wind Turbines," *J. Fluids Engineering*, 2002, 124, pp. 393-399

[24] Frandsen, S., Barthelmie, R., Pryor, S., Rathmann, O., Larsen, S. and Højstrup, J., "Analytical Modelling of Wind Speed Deficit in Large Offshore Wind Farms," *Wind Energy*, 2006, 9, pp. 39-53

[25] Stefanatos, N., Voutsinas, S., Rados, K. and Zervos, A. "A Combined Experimental and Numerical investigation of Wake Effects in Complex Terrain," *Proceedings of 1994 EWEC*, Thessaloniki

[26] Chaviaropoulos, P. K. and Douvikas, D. I., "Mean-flow-field Simulations over Complex Terrain Using a 3D Reynolds Averaged Navier–Stokes Solver," *Proceedings of ECCOMAS '98*, 1998, Vol. I, Part II, pp. 842-848

[27] Wilcox, D. C., *Turbulence Modelling for CFD*, DCW Industries Inc., La Canada, California, 1993, IBSN 0-9636051-0-0

[28] Launder, B. E. and Spalding, D B., "The Numerical Computation of Turbulent Flows,'" *Computer Methods in Applied Mechanics and Engineering*, Vol. 3, pp. 269-289. ,1974

[29] Counihan, J., "Adiabatic Atnospheric Boundary Layer: a Review and Analysis of Data from the Period 1880-1972," *Atmos. Environ.*, 1975, 9, pp. 871-905

[30] Panofsky, H. A. and Dutton, J. A., *Atmospheric Turbulence*, Wiley Interscience, New York, 1984, 397pp

[31] Stull, R. B., *An Introduction to Boundary Layer Meteorology*, Kluwer Academic Publishers, Dordrecht, 1988, 666pp

[32] Frenzen, P., Vogel, C., "On the Magnitude and Apparent Range of Variation of the Von Karman constant in the Atmospheric Surface Layer," *Boundary Layer Meteorology*, 72, pp. 371-392

[33] Garrat, J. R., "Review of Drag Coefficients over Oceans and Continents," *Mon. Wea. Rev.*, 1977, 105, pp. 915-929

[34] Townsend, A. A., The Structure of Turbulent Shear Flow, 2nd ed., Cambridge University Press, Cambridge, 1976

Appendix: Relation between inflow turbulence intensity and roughness length.

The turbulent kinetic energy, *k*, is defined as:

$$k = 0.5\left(\sigma_x^2 + \sigma_y^2 + \sigma_z^2\right), \qquad (16)$$

where σ_x, σ_y and σ_z are the standard deviations of the velocity fluctuations in directions *x, y, z* respectively. Taking into account the anisotropy of turbulence, $\sigma_y / \sigma_x = 0.8$ and $\sigma_z / \sigma_x = 0.5$ at flat terrain conditions, and Eq. (16) becomes:

$$k = 0.945\,\sigma_x^2 \ . \qquad (17)$$

Combining Eqs. (14) and (17) results in the relationship:

$$\sigma_x = 2.4135\,u_* \qquad (18)$$

The inflow turbulence intensity at hub height, TI_{in}, is defined as $TI_{in} = \sigma_x / U_{in}$ with U_{in} being the local inflow wind speed. Using this definition, Eq. (18) can be written as:

$$\frac{U_{in}}{u_*} = \frac{2.4135}{TI_{in}} \qquad (19)$$

By substituting equation (19) into the logarithmic inflow velocity profile given by equation (11), it follows that:

$$\frac{2.4135}{TI_{in}} = \frac{1}{K} ln\left(\frac{z_{hub}}{z_0}\right)$$

or

$$z_0 = z_{hub}\,exp\left(-0.9895 / TI_{in}\right) \qquad (20)$$

which relates the inflow turbulence intensity TI_{in} at hub height z_{hub} with the roughness length z_0.